



Preliminary methodology assessment for PEMFC durability testing in transport applications[☆]

Sara Tamburello^{a, ID, *}, Marco Russo Cirillo^{b, ID}, Yurii Yakovlev^{c, ID}, Iva Matolínová^{c, ID}, Rodolfo Taccani^b, Andrea Coraddu^{a, ID}, Marco Bogar^{b, ID}, Lindert van Biert^{a, ID}

^a Department of Maritime & Transport Technology, Faculty of Mechanical Engineering, Delft University of Technology, Mekelweg 2, 2628 CD, Delft, The Netherlands

^b Department of Engineering and Architecture, University of Trieste, Via Alfonso Valerio 6/1, 34127, Trieste, Italy

^c Department of Surface and Plasma Science, Faculty of Mathematics and Physics, Charles University, V Holešovičkách 2, 180 00, Prague 8, Czech Republic

ARTICLE INFO

Keywords:

Maritime PEMFC
Durability test
Ship operating cycle
Electrochemical analysis

ABSTRACT

As Polymer Electrolyte Membrane Fuel Cells (PEMFCs) emerge as a promising technology for transport decarbonization, the development of durability assessment protocols tailored to specific applications, such as maritime operations, is becoming relevant for the identification of stressors and lifetime enhancement. This study presents a preliminary experimental campaign aimed at introducing a methodology to assess the degradation of PEMFCs subjected to Accelerated Stress Test (AST). In particular, the methodology encompasses the utilization of electrochemical characterization and, in this work, the fuel cell operating profile has been chosen to mimic the operation of a small passenger vessel. The tests were carried out on two single Membrane Electrode Assemblies (MEAs) for 500 h. One membrane was subjected to the AST, and a second sample, tested under constant load operation, served as a reference. Periodic electrochemical characterization was conducted to assess performance degradation through polarization curves, electrochemical impedance spectroscopy, and cyclic voltammetry. The electrochemical analysis of degradation was conducted through a dual-method approach combining model-free and model-based methods for impedance analysis, as well as catalyst active area evaluation from voltammograms. Results show that the dynamic operation characteristic of the passenger ferry increases degradation compared to constant operation, evidenced by increased ohmic and interfacial resistances and losses in catalyst active area. This work provides a framework for developing application-specific durability protocols, enriched with multi-method diagnostic approaches to assess PEMFC degradation under realistic maritime conditions. Such methodologies support the development of durability enhancement strategies tailored to maritime applications, allowing a broader application of the technology in the sector.

1. Introduction

In recent years, the maritime sector has faced increasing pressure to reduce its environmental impact [1]. Polymer Electrolyte Membrane Fuel Cells (PEMFCs) have emerged as a promising zero-emission alternative to conventional engines for primary power generation [2]. With respect to other fuel cell technologies, PEMFCs are characterized by high specific power and power density, high electrical efficiency, fast start-up time, and effective transient response [3,4]. Already used at the commercial level in the automotive or railway sector as a powertrain, PEMFCs dominate ongoing fuel cell demonstration projects for maritime energy systems as well, accounting for 75% of the applications in fuel cell projects developed between 2001 and 2024 [5].

Most PEMFC-based propulsion systems for ships adopt a hybrid configuration in which an Energy Storage System (ESS) is installed to enable load decoupling, and to optimize component sizing and operation [6]. This configuration offers an emission-free solution that is particularly suitable for decarbonizing small and medium-sized vessels, such as ferries and tugs [7]. Nonetheless, the widespread adoption of PEMFCs in ship energy systems is hindered by their limited durability, as their performance degrades over time, resulting in shorter operational lifetimes and increased hydrogen consumption in the late stages of life, thereby increasing the operational costs [8,9]. Therefore, understanding and predicting the long-term behavior of PEMFCs under

[☆] This article is part of a Special issue entitled: 'EFCF2025' published in Electrochimica Acta.

* Corresponding author.

E-mail address: s.tamburello-1@tudelft.nl (S. Tamburello).

real-world operating conditions is crucial for estimating their lifetime and enhancing durability.

To address durability challenges and better understand the underlying degradation mechanisms, a series of Accelerated Stress Tests (ASTs) targeting specific PEMFC components has been developed to investigate how degradation mechanisms affect various materials and designs [10]. However, these protocols are not suitable for evaluating the overall PEMFC lifetime under application-specific operating conditions since they only focus on individual components and their use might provide partial results when applied at a stack level, where degradation develops following more complex pathways.

Drive-cycle durability protocols are the most suitable approach for assessing fuel cell durability in mobility applications at the cell and stack level. Drive-cycle-based ASTs have been primarily developed for automotive applications and are based on a set of assumptions regarding the typical operation of fuel-cell-powered vehicles [11]. In this case, a drive-cycle protocol simulates the actual road operation as a rational combination of different typical conditions such as start-up and shut-down, idling, high load, and load cycling. For example, the cycling protocol issued by the Department of Energy (DOE) of the United States of America reflects the power demand of vehicles operating in typical American urban environments, featuring higher speeds and more frequent elevation changes [12]. To simulate this operation, a single testing cycle includes open circuit voltage (OCV), low current, medium current, and high current phases [13]. In contrast, the EU harmonized test protocol for PEMFC single-cell testing in automotive applications is based on the New European Driving Cycle (NEDC), which reflects both typical urban driving conditions in European cities, characterized by low engine loads and frequent start and stops, and extra-urban driving cycle with fewer start and stops and higher loads [14]. The NEDC includes startup and shutdown, idling, partial power running, full power running, and dynamic loading running.

Automotive-derived ASTs are, however, not representative of maritime applications. Ships exhibit a wide range of load profiles depending on the vessel type, and load profile can differ significantly from those of road vehicles. For automotive PEMFC, dynamic load is the most frequently experienced condition according to its need for accelerating and braking to deal with different traffic conditions during urban road driving. In maritime, instead, dynamic conditions vary depending on the vessel application: larger ships exhibit more stable load distributions, while smaller vessels, more suited for PEMFC applications, generally experience higher load variability [15]. Unlike cars, ships experience substantial power fluctuations even at constant speeds due to external factors such as hull fouling, fuel and cargo variations, and maneuvering conditions [16]. A typical vessel's power demand, even with thruster power management and speed control, can vary by up to 40% of nominal power within 10 s [15]. Automotive studies indicate that 56.6% of PEMFC performance degradation results from transient load fluctuations [17]. Given the even greater load variability of ships, their power demands on PEMFCs could result in degradation rates differing from automotive applications. Conversely, while start-stop cycles statistically occur 7 times per hour for a road vehicle, their frequency is lower for ships with longer sailing missions [10]. Additionally, once a ship stops at port, power is still needed for cargo operations and onboard hotel loads, minimizing idling and open-circuit voltage conditions. These distinct operating conditions can affect degradation differently from typical automotive operation.

Due to these distinct requirements, durability protocols tailored to maritime applications have recently started to be studied. Choi et al. [18] developed a maritime durability protocol designed to mimic the operation of a small research vessel on a single Membrane Electrode Assembly (MEA) over 300 operating hours, which proved to be harsher than the DOE protocol. However, the proposed protocol does not cover all types of ships, and further work is required to test the effect of various operational profiles reflecting the diversity of ship types. Moreover, protocols at the MEA level require accurate analysis

of the electrochemical processes to identify the underlying degradation mechanisms of key components related to specific maritime dynamics. Such electrochemically rooted degradation analyses are still lacking in the context of maritime-specific durability studies.

To address these gaps, this work presents a methodology to evaluate degradation of PEMFC MEAs due to a novel transient load cycle, mimicking the operation of the hydrogen-powered FCS Alsterwasser, a passenger ferry currently operating in Hamburg [7,19]. The protocol was applied to a single MEA over 500 operating hours, with electrochemical characterization carried out via polarization curves, Electrochemical Impedance Spectroscopy (EIS), and Cyclic Voltammetry (CV). As a reference, degradation was monitored on a second MEA aged under constant load within the same time frame. The methodology integrates a detailed electrochemical analysis, including EIS modeling through both Equivalent Circuit Model (ECM) fitting and the Distribution of Relaxation Times (DRT) approach, as well as Electrochemical Active Surface Area (ECSA) evaluation from voltammograms. While the test protocol is based on a specific vessel, the methodology represents an initial step toward a framework for standardized durability protocols tailored to maritime applications, addressing a critical gap that is necessary to parallel progress in other sectors. Moreover, the electrochemically rooted approach enables a deeper understanding of degradation mechanisms associated with dynamic maritime operation, which is essential for the development of durability enhancement strategies such as health-aware energy management.

2. Experimental

2.1. Materials

Two MEAs of 4 cm² active area were composed of a self-fabricated Catalyst Coated Membrane (CCM) loaded with Pt/Vulcan catalyst layer. CCMs were prepared by ultrasonic spraying of a catalyst ink on the surface of an ionomeric reinforced membrane (Nafion[®] NR212, FuelCellStore) by means of a CNC controlled system (ExactaCoat, SonoTek), as previously detailed in [20,21]. Pt/C catalyst particles (Pt on Vulcan XC-72R, 40%, FuelCellStore), ionomer dispersion D521 (5% 1100 EW, FuelCellStore), and isopropanol/acetone solvent (1:1 ratio) were ultrasonically mixed for 20 min at 75% of power with a 0.5/0.5 on/off cycle using the HD-3100 sonicator (Bandeling SonoPulse). Ink composition was adjusted to get I/C ratio of 0.6 in the dry catalyst layer [20]. The membrane was secured on a hot-bed (60°C) during the spraying process. The active catalyst area was filled with a serpentine pattern, resulting in the deposition of 0.025 mgPt/cm² per layer. After each layer, the machine was stopped for 30 s to ensure complete solvent evaporation. The coating process was repeated to achieve a catalyst load of 0.5 mg/cm² on the cathode and 0.1 mg/cm² on the anode. Commercial Sigracet 29BC was used as a gas diffusion layer.

2.2. Durability protocol

The two MEAs were tested under galvanostatic control for a total duration of 500 h, using a home-built test station equipped with a Biologic SP-150 potentiostat and a VMP-3 booster. Graphite bipolar plates with a single-serpentine flow field and an active area of 4 cm² were used for fuel cell measurements. Cell temperature was set to 70°C, hydrogen and air flow rates were set to 1 bar gauge pressure and 80% relative humidity by setting the humidifier dew point at 65°C, while stoichiometry was maintained at a constant value of 2, based on the maximum operating current of each test. A schematic of the testing protocol is shown in Fig. 1. Before the actual operating test, a break-in procedure was performed, consisting of constant operation at 0.5 A/cm² until stable performance was reached for both MEAs. The first sample (MEA AST) was tested under the dynamic ship operating cycle repeated over the total test duration, while the second sample (MEA Ref) was tested under constant load, at the operating point of

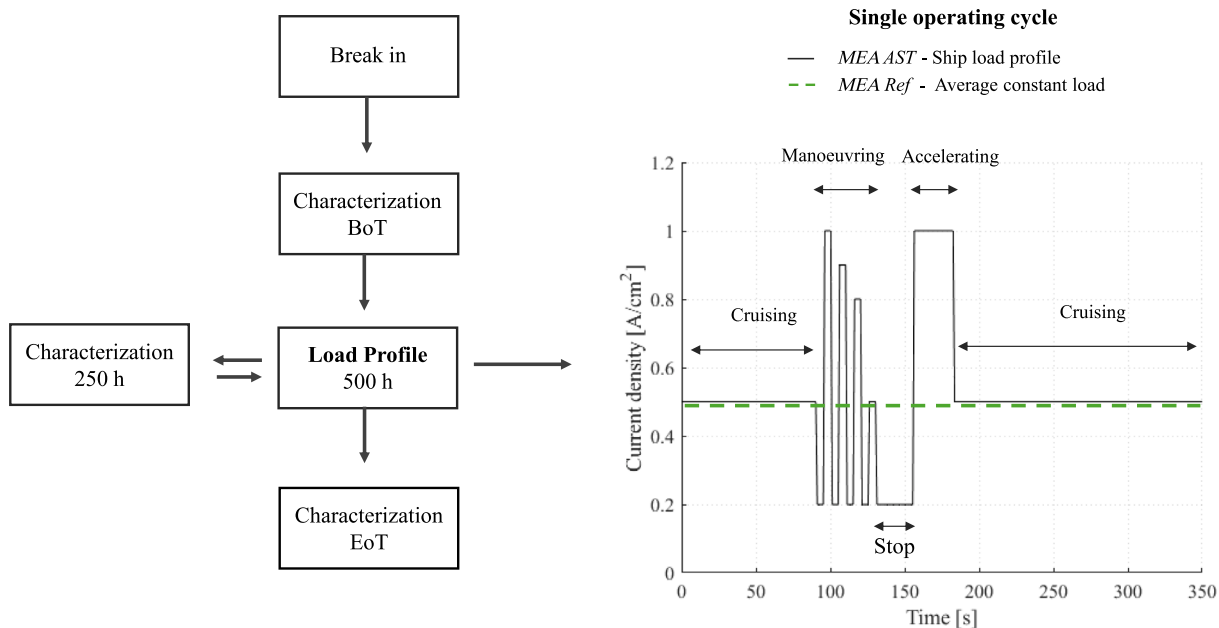


Fig. 1. Schematic of the testing protocol procedure and single operating cycles for *MEA AST*, operated under the ship load profile derived from the Alsterwasser vessel, and for *MEA Ref*, operated under constant average load.

0.5 A/cm², corresponding to the average load of the ship load profile. This also ensures that the total charge per protocol is equivalent and equal to 700 C for *MEA AST* and *MEA Ref*.

The ship load profile for the durability protocol has been designed by elaborating to the power profile of a small passenger fuel cell vessel, which is equipped with two PEMFC systems of 48 kW each, and a 360 Ah/560 V lead gel battery and its operational profile has considerable variation in power requirements, including propulsion and auxiliary power [22]. The power profile has been simplified into a single 350-second cycle to be repeated over time, and normalized in terms of current density. This load cycle simulates the vessel's operating phases, including critical high load and load cycling, to evaluate their impact on the PEMFC degradation. Specifically, the simplified load cycle consists of two cruising phases with constant operation at 0.5 A/cm² for 90 s and 170 s, respectively; a maneuvering phase involving load cycling between a lower operating point of 0.2 A/cm² and upper operating points of 1.0, 0.9, 0.8, and 0.5 A/cm² for a total duration of 40 s; a stop phase at the constant minimum operating point of 0.2 A/cm² for 25 s; and an acceleration phase with constant operation at 1.0 A/cm² for 25 s. As operating data of the actual PEMFC system used onboard were not available, the chosen profile derived from load demand does not replicate in terms of current density and voltage the one recorded on the actual vessel. Moreover, voltage levels lower than those normally encountered in commercial fuel cells were allowed in order to amplify degradation phenomena in the AST. The voltage response of *MEA AST* is provided in supplementary material, Figure S1.

Electrochemical characterizations were performed at the Beginning of Test (BoT), after 250 h of operation, and at the End of Test (EoT). Polarization curves were recorded under linear sweep voltammetry from OCV to 0.3 V, with a step of 1 mV/s. EIS were recorded in galvanostatic mode under stationary operation at 0.2 A/cm², with a 5% amplitude of disturbance current, from 10 kHz to 0.1 Hz, and with 10 points per decade. The EIS operating point of 0.2 A/cm² guarantees a proper activation state of the catalyst, thereby avoiding mass transport limitations and ensuring stability of measurements. While both charge transfer and ohmic processes can be captured at this operating point, mass transport limitations and water management issues are voluntarily avoided, allowing DRT and ECM analysis to capture actual catalyst and electrolyte degradation. CVs were recorded in hydrogen–nitrogen atmosphere from 0 to 1.0 V at 100 mV/s slew rate.

2.3. Electrochemical analysis

EIS spectra were analyzed by combining both model-free [23] and model-based methods [24]. Firstly, DRT analysis was performed using the package DRT tools for MATLAB [25,26]. This method enables the identification of electrochemical processes via the relaxation times distribution [27]. In DRT analysis, the complex impedance is associated with the relaxation time constant by means of:

$$Z(f) = R_0 + \int_0^{\infty} \frac{\gamma(\ln \tau)}{1 + i2\pi f\tau} d(\ln \tau)$$

where R_0 is the ohmic resistance, while the integral term is known as the polarization impedance. Here, τ denotes the relaxation time, f the frequency, and $\gamma(\ln \tau)$ the distribution relaxation times function. To determine the solution of $\gamma(\ln \tau)$, the regularized regression method proposed by Wan et al. [26] was followed, within the piece-wise linear approximation method. The regularization parameter (λ) was set to 10^{-3} , which is recognized in literature as a suitable trade-off between accuracy enhancement and disturbance minimization [28–30]. As a result of computation, a series of peaks composes the DRT spectrum, expressed as a function of the relaxation time: each of the peaks corresponds to a specific process evolving within the MEA, and the resistance associated with each process is represented by the peak area.

In line with a recent approach to EIS analysis [28], DRT results served as a basis for the subsequent ECM analysis. This methodology helps in developing the equivalent circuit to be used for ECM analysis, as different circuit configurations may produce similar impedance spectra, potentially leading to misinterpretation [31]. Moreover, this approach enhances fitting accuracy, which is particularly sensitive to the initial parameter estimates [23]. The ECM was constructed based on the processes identified through the DRT analysis: a single resistance was used in series with three R–C parallel elements, as shown in Fig. 2 and later detailed in Section 3.1. ECM fitting was carried out using the Zfit function in MATLAB [32], which employs nonlinear least-squares optimization to minimize the difference between the measured and simulated impedance in the complex domain. Initial values for the ECM parameters were derived from the time constants, resistances, and capacitances obtained through DRT analysis.

Finally, voltammograms were used to determine the specific ECSA by the ratio Q/GL , where Q (C/cm²) represents the charge from

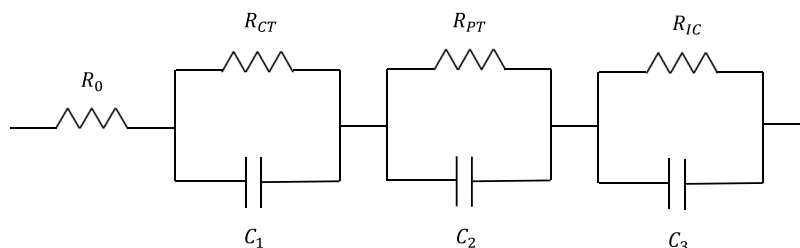


Fig. 2. Equivalent circuit defined for the ECM analysis.

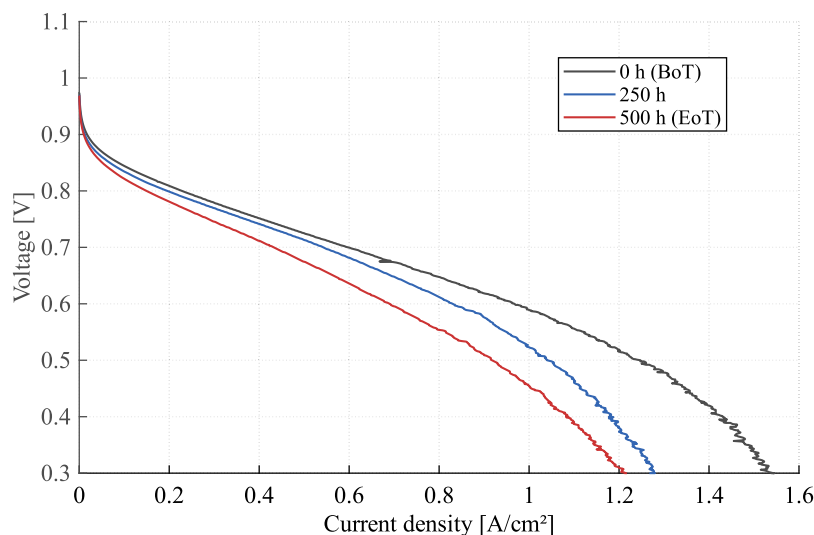


Fig. 3. Polarization curve evolution for MEA AST.

hydrogen desorption, G is the specific charge required to oxidize a monolayer of hydrogen on platinum (typically taken as $210 \mu\text{C}/\text{cm}^2$), and L (g/cm^2) is the platinum loading in grams per square centimeter. Voltammograms were also employed to compute both the hydrogen crossover current (I_{cross}) and the double-layer capacitance (C_{dl}), starting from the current values retrieved in the plateau region from the forward and backward voltage scans [33], from which hydrogen crossover current and double-layer capacitance could be retrieved: $I = I_{\text{cross}} + I_{dl} = I_{\text{cross}} + C_{dl} \frac{dV}{dt}$.

3. Results and discussion

The performance of the MEAs operated under a ship-load profile (MEA AST) and under constant load (MEA Ref) was compared. Unfortunately, polarization curves of MEA Ref were measured during unstable conditions at higher operating current and could not be used for degradation comparison. Consequently, the degradation analysis focuses on the EIS and CV results. Fig. 3 shows the full polarization curve evolution for MEA AST.

3.1. EIS analysis

Impedance spectra for the two tests, and the analysis performed using the combined DRT-based and ECM approach described in the previous section, are presented in Fig. 4. Nyquist plots for MEA AST, shown in Fig. 4(a), exhibit a noticeable growth in both the high frequency intercept and the diameter of the semicircle over time, indicating increases in both ohmic and charge transfer resistance. In contrast, MEA Ref, shown in Fig. 4(b), tested under constant average load, shows a more modest and gradual change in impedance response. The semicircle diameter increases only slightly, and the high frequency

intercept remains relatively stable, suggesting slower degradation of the charge transfer processes and relatively stable membrane resistance.

DRT analysis, shown in Figs. 4(c) and 4(d) for MEA AST and MEA Ref, respectively, revealed three well-separated peaks, each associated with a distinct physical process. As spectra were recorded at a low current density value of $0.2 \text{ A}/\text{cm}^2$, low-frequency peaks characteristic of mass transport phenomena are excluded from the analysis. By referring to other studies present in literature [28,34], and by comparing their evolution during the stress tests, peaks were mapped as follows: the first peak (P1) was attributed to charge transfer resistance (R_{CT}) associated with the Oxygen Reduction Reaction (ORR), the second peak (P2) was linked to proton transport resistance (R_{PT}) within the ionomer of the cathode catalyst layer, while the third peak (P3) was related to the charge transport resistance (R_{IC}) at the electrode-membrane interface [23].

Peak evolution over the testing period was found to be different for the two samples. When the novel AST was applied, all three peaks underwent substantial changes, reflecting pronounced electrochemical degradation. P1 shifts slightly toward higher frequency and exhibits a strong increase in amplitude after 250 h, corresponding to an increase in R_{CT} . By the end of the test, P1 amplitude decreases, but the peak broadens, suggesting a wider distribution of relaxation times, likely due to catalyst layer degradation. Such evolution could be due to a change of ECSA, as the operating voltage over the test switches iteratively from 0.4 V to 0.8 V, causing continuous reduction and oxidation of platinum nanoparticles, which has been shown to trigger catalyst nanoparticle growth [35–37]. P2 retains a consistent peak position (characteristic frequency) but increases in amplitude. The corresponding increase in process resistance suggests the occurrence of degradation of proton conduction pathways. Such a result would be in agreement with the change in catalyst particle size distribution, in particular with the dissolution of the ionomer surrounding the catalyst nanoparticles. Finally, P3 shows

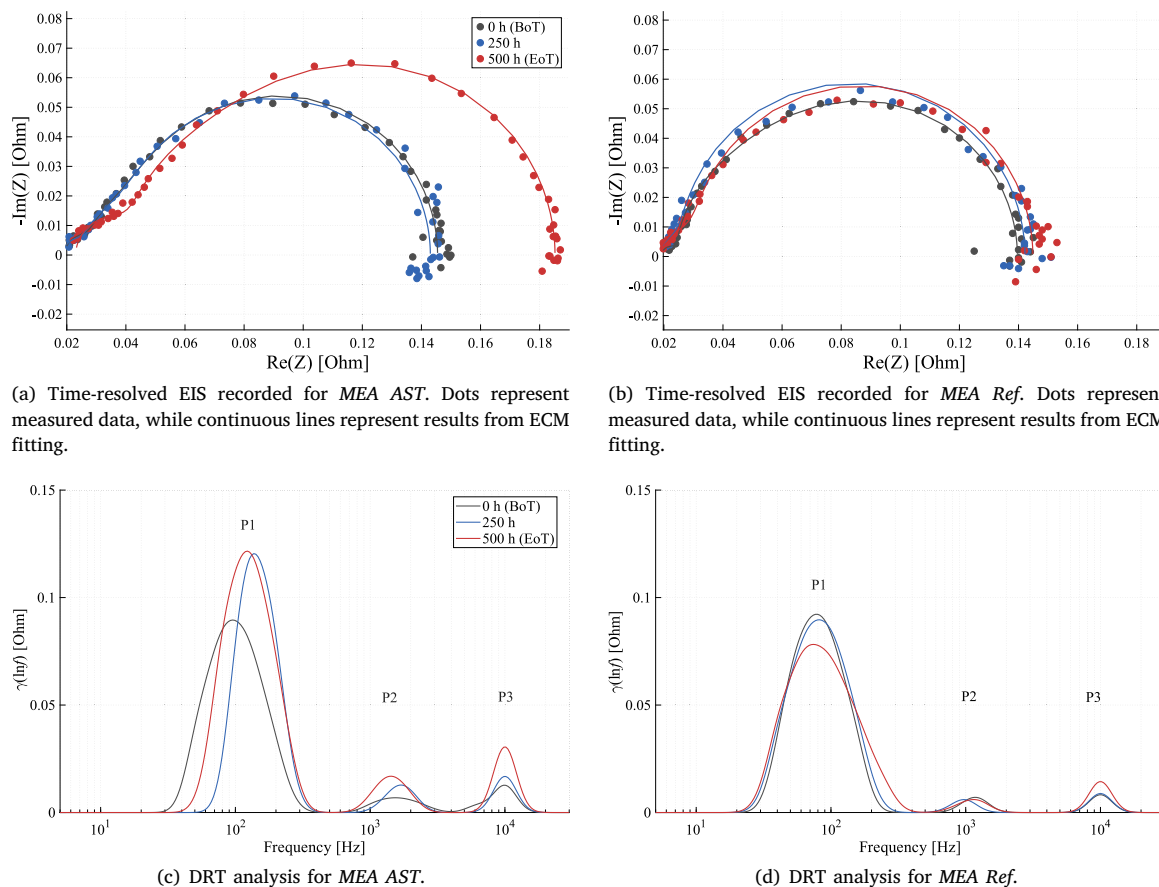


Fig. 4. EIS analysis for the two tested samples.

a stable frequency but a significant amplitude increase, especially in the second half of the test, indicating a possible increase in interfacial resistance between the electrode and the polymer membrane, meaning that proton transfer between the catalyst layer and the membrane became less efficient. This increase could arise from catalyst layer delamination due to mechanical stress or membrane swelling, but can also be influenced by interfacial wetting properties, such as contact angle and the viscosity of phosphoric acid [38]. Consequently, reduced hydration of the ionomer at the interface could also contribute to the observed rise in interfacial resistance. In contrast, the peak evolution for *MEA Ref* remains relatively limited. All three peaks maintain consistent frequencies and only minor amplitude changes throughout the testing protocol. Specifically, P1 exhibits only a marginal increase in amplitude without broadening, suggesting less pronounced changes in ORR kinetics with respect to *MEA AST*. P2 and P3 remain notably stable in both amplitude and position, indicating that proton transport and membrane–electrode interface degradation were also less significant in *MEA Ref*.

Based on DRT analysis, the equivalent circuit consists of an ohmic resistance R_0 , representing the resistance of the proton exchange membrane, in series with three parallel R–C branches, as shown as the insert in Fig. 2. Each branch corresponds to a distinct electrochemical process identified through the DRT peaks. Results of the ECM fittings obtained for the EIS data for *MEA AST* and *MEA Ref* are shown in Figs. 4(a) and 4(b), respectively, as continuous lines over the measured data. The ECM provides high fitting accuracy across all datasets, with values of the coefficient of determination (R^2) exceeding 0.96 for both the real and imaginary components, as detailed in Supplementary Material (Table S1).

The evolution of the resistance values obtained via DRT and ECM analyses for *MEA AST* and *MEA Ref* are compared in Fig. 5. For *MEA*

AST, the ohmic resistance R_0 shows a consistent increase in both DRT and ECM analysis, in the order of 15%–20%, which could be due to membrane hydration instability and chemical degradation of the membrane affecting its proton conductivity. In dynamic operations, such as those of ferries, frequent changes in current demand result in not constant rate of produced water [39,40]. These fluctuations can cause transient drying of the membrane, especially during high-load phases when the anode and cathode are rapidly depleted of humidified gases. Moreover, dynamic loads can cause cyclic mechanical fatigue that challenges the interfaces between layers, such as membrane–catalyst or catalyst–gas diffusion layer, causing loss of contact integrity or localized delamination that increases contact resistance [40]. Repeated load cycling induces frequent thermal and hydration expansion–contraction cycles in the membrane, generating mechanical stress that can eventually lead to micro-cracking or pinhole formation [41]. Since the abrupt performance drops typically associated with crack or pinhole formation did not occur during the load cycling test for *MEA AST*, we assume that mechanical degradation of the membrane was limited and did not result in significant defect formation. To further support this hypothesis, we verified that the hydrogen crossover current did not increase over the test, confirming that membrane degradation did not result in the formation of pinholes or cracks. Specifically, the crossover current at the EoT for *MEA AST* resulted to be around 0.7 mA/cm², which is aligned with standard crossover values of fresh NR212 [42].

Both DRT and ECM analyses show a slight decrease in the high frequency resistance R_0 for *MEA Ref*. While counterintuitive, this trend may reflect improved membrane hydration over time due to sustained steady-state operation, which avoids the humidity fluctuations typical of dynamic loading [43]. Under constant current conditions, water generation and distribution tend to reach a more stable equilibrium,

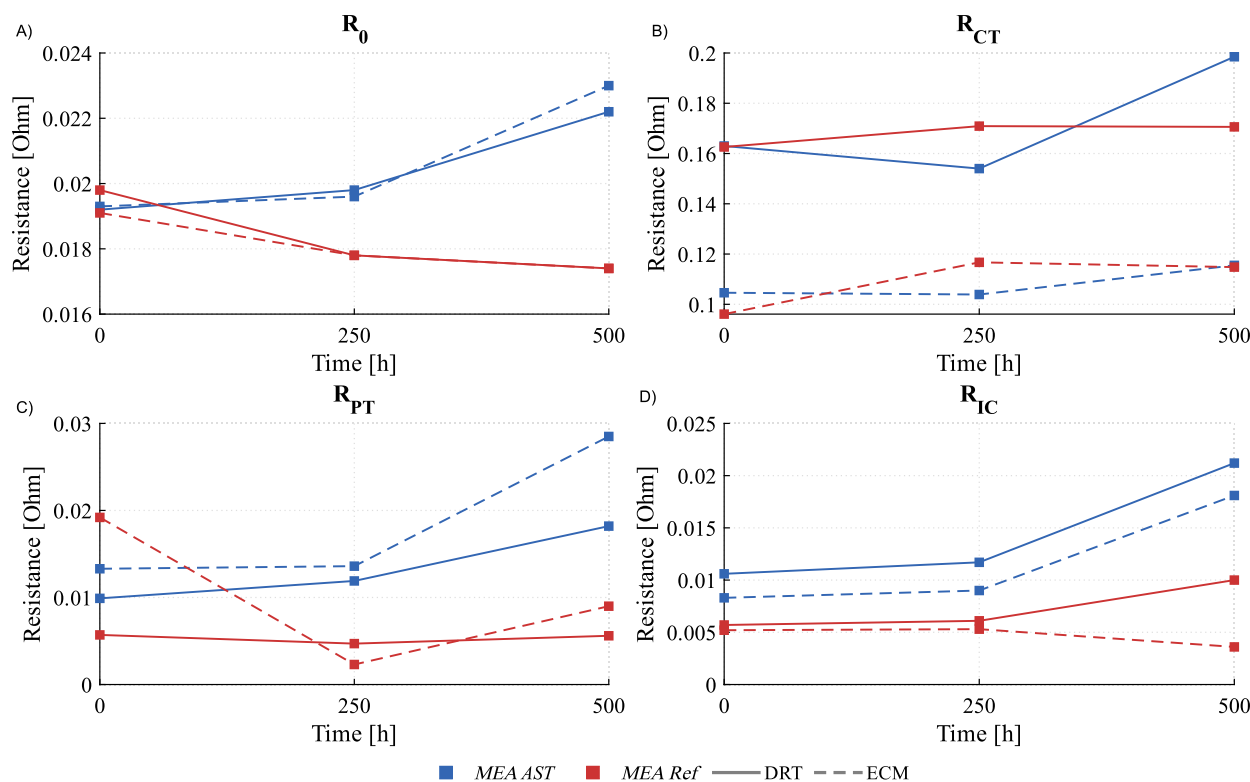


Fig. 5. Evolution of resistance parameters over time for MEA AST and MEA Ref, as evaluated by DRT and ECM analysis.

potentially enhancing membrane conductivity and reducing contact resistance at the membrane–electrode interface [44].

For the mid-frequency arc, represented by R_{CT} , DRT and ECM methods capture a resistance increase for both MEA AST and MEA Ref. This indicates a reduction in ORR kinetics, most likely due to catalyst layer degradation such as Pt dissolution, agglomeration, or detachment, ionomer degradation, flooding, or dehydration of the catalyst layer, and carbon support corrosion [45–47]. For MEA AST, DRT shows a greater R_{CT} increase than ECM, which might reflect its greater sensitivity to overlapping time constants and subtle shifts in electrochemical kinetics that can be masked or smeared out in ECM fitting. For MEA Ref instead, DRT shows a more moderate R_{CT} decrease than ECM, which is more in line with a slower ORR decay expected for constant load operation.

Larger magnitude discrepancies arise for the low-frequency resistances R_{PT} and R_{IC} . Considering MEA AST, although both methods agree on the increasing trend, the divergence in absolute values suggests ECM may overfit or misattribute low-frequency features. The increase in R_{PT} over the test indicates worsening proton conductivity within the catalyst layer, likely due to ionomer dehydration, chemical degradation due to radical attack, delamination, and redistribution. Similar increased ionic resistance in the catalyst layer has been observed after long-term operation or ASTs, correlating with ionomer degradation, thinning, and decomposition [48,49]. The increase in R_{IC} indicates degradation at the electrode–membrane interface. Under dynamic operating conditions, frequent fluctuations in current demand induce variations in thermal and humidity levels, leading to repetitive hydration–dehydration and thermal expansion–contraction cycles. These mechanical and chemical stressors can weaken the physical and ionic contact at the interface, resulting in delamination, microcracks, or mechanical creep [50].

For MEA Ref, discrepancies between the methods in both R_{PT} and R_{IC} evolution make the interpretation particularly challenging. According to the DRT, R_{PT} remains almost constant by EoT, while R_{IC} exhibits a clear increase over the duration of the test, with a net rise of approximately 73.95% at the EoT. The ECM fitting, instead,

yields a decrease in both R_{PT} and R_{IC} , which contradicts the expected degradation. Nonetheless, results might be affected by limitations in least square fitting approach in disentangling the contributions of the less intense process (charge transport at the catalyst–ionomer interface) with respect to the prevailing one (ORR) at high-frequencies [28]. Therefore, we rely on DRT for the evaluation of R_{PT} and R_{IC} trends. To further support this hypothesis, the double-layer capacitance C_{dl} was evaluated from CVs as explained in Section 2.3. The decrease in double-layer capacitance (Fig. S2) provides an independent indicator supporting the DRT-derived trends of increasing R_{PT} and R_{IC} for both MEA AST and MEA Ref, and is found in agreement with the observed loss of ECSA loss. A reduction in C_{dl} typically reflects a loss of ECSA, ionomer thinning and/or detachments, and/or reduced wetting of the catalyst layer. These degradation pathways can cause an increase in both proton transport resistance in the ionomer of the catalyst layer (R_{PT}), and interfacial charge-transfer resistance at the membrane–electrode interface (R_{IC}) [51].

3.1.1. Discussion on methods

The combined use of DRT and ECM analyses enables a more comprehensive interpretation of the impedance spectra and degradation behavior of the tested MEAs, as well as a direct comparison of the two methods. The DRT provides a robust separation of overlapping electrochemical processes based on their relaxation times, offering higher sensitivity in parameter identification, especially in the low-frequency domain where transport and interfacial phenomena dominate [23].

DRT proved particularly valuable for evaluating parameters corresponding to proton transport in the ionomer phase and interfacial contact resistance. In contrast, the ECM approach showed significant limitations in these frequency regions, as observed in other studies [28]. Despite being guided by DRT for model structure and initial estimates, ECM frequently underestimates or overestimates resistance values or predicted trends inconsistent with expected physical behavior, suggesting an inherent rigidity in the circuit-based fitting method. ECM proved to be more effective at resolving high frequency features, even

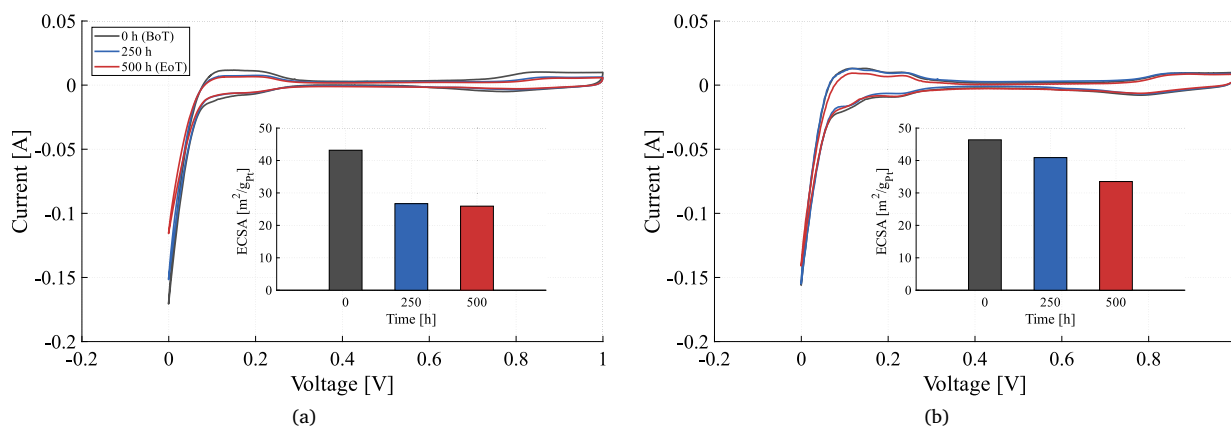


Fig. 6. Voltammograms and ECSA calculation for *MEA AST* (A) and *MEA Ref* (B) over the AST.

though its accuracy heavily depends on appropriate model selection and initial parameter estimation. This combined approach showed the DRT capability to accurately identify key electrochemical processes, guiding the definition of an ECM with clearer physical correspondence to the observed phenomena. However, the analysis showed the limitations embedded in the traditional ECM method, proving that alternative model-free methods, such as DRT, are necessary for accurate EIS analysis.

3.2. CV analysis

Electrochemical characterization was completed by comparing the evolution of CV in the two stress tests applied, as shown in Fig. 6. The voltammogram of *MEA AST* shows a substantial reduction in the hydrogen adsorption and desorption regions (between 0.05 and 0.4 V), indicating a marked decline in platinum surface activity over the test. This loss of active sites was quantitatively evaluated by ECSA calculation, which resulted in a 38% and 40% drop within the first 250 and 500 h of test, respectively, highlighting that ECSA loss mainly evolves in the initial phases of operation (suggesting an exponential-like decay), likely driven by rapid Pt dissolution and agglomeration under dynamic operating conditions, resulting in an increase of Pt particle size and distribution. This result is in good agreement with other works proving that catalyst degradation under dynamic operation happens at a fast rate in early stages and is coupled with changes in particle size and distribution due to coalescence and Ostwald ripening [35,52,53].

In contrast, *MEA Ref* exhibited a more stable CV profile, with the hydrogen adsorption/desorption region better preserved throughout the test. The ECSA in this case declined by only 12% in the first half of the test and by 28% at the end, following a more linear degradation trend. This steady decline reflects a slower rate of catalyst deactivation over time associated with constant operation, in which degradation mechanisms caused by Pt oxidation and reduction are not triggered [45]. These differences imply that the ship load cycle conditions imposed on *MEA AST* likely intensified degradation phenomena such as platinum oxidation and reduction, dissolution and agglomeration, coalescence, and potential catalyst detachment [45]. Meanwhile, the more moderate decline in *MEA Ref* tested at constant load suggests that under less aggressive or constant load conditions, catalyst degradation mechanisms progress at a slower rate.

The trends characterizing ECSA variations are found in agreement with the trends outlined by mid-frequency resistance R_{CT} increase for both of the MEAs. While ECSA indicates the actual catalyst active area (available to sustain the redox reactions), R_{CT} reflects the catalyst efficacy in sustaining the ORR reaction, a process that depends on both ECSA and the electrochemical reaction rate [54]. For *MEA AST*, R_{CT} increased by 20.1% according to DRT and 10.4% according to ECM,

showing an increasing trend consistent with the observed ECSA loss of 40%. Similarly, for *MEA Ref*, the correlation follows a similar pattern: ECSA dropped by 28%, and the DRT analysis indicates a ~5% increase in R_{CT} . Given these observed trends, we conclude that ECSA is the primary factor driving the increase in R_{CT} for both *MEA AST* and *MEA Ref*. These observations are consistent with R_{CT} and ECSA trends observed in other catalyst degradation studies [55].

4. Conclusions

This study proposes a methodology to assess degradation caused by a novel AST designed to represent the specific transient load profile of a hydrogen-powered passenger ferry, using a combined DRT and ECM method for EIS analysis, and ECSA evaluation from CVs.

Results show that the application of the ship-inspired dynamic load leads to a reduction in ORR kinetics and to an increase in proton-transport resistances across the membrane, the catalyst layer, and the membrane–electrode interface. The rise in membrane resistance is primarily attributed to unstable hydration and chemical degradation driven by the rapid transients typical of small-vessel operation. Since no increase in hydrogen crossover current was observed, it was assumed that no harsh degradation phenomena, such as pinhole or crack formation, affected the membrane over the investigated timeframe. This is consistent with the fact that maritime PEMFCs experience fewer high-impact events typical of automotive operation, such as start-ups and shut-downs, resulting in slower rates of membrane chemical and mechanical degradation, as well as limited carbon corrosion.

In contrast, the fast load dynamics characteristic of the ferry operation can accelerate catalyst layer degradation by promoting Pt oxidation–reduction, dissolution, agglomeration, and detachment, as well as ionomer degradation, increased interfacial contact resistance, and water management instabilities. The observed decline in ORR activity is therefore most plausibly linked to catalyst-layer degradation mechanisms, which is consistent with the measured ECSA and double-layer capacitance decrease.

These findings show how degradation can develop in PEMFCs operating as powertrains for small vessels. While both automotive and maritime operations are characterized by dynamic load-induced stressors, the frequency and occurrence of these phenomena can significantly differ depending on the application, affecting degradation in different measures. In particular, propulsion systems of small vessels, such as ferries or tugs, often experience longer-duration partial loads punctuated by sharp transients during docking, turning, or maneuvering, unlike the relatively brief and more frequent transients in road vehicles. Additionally, external factors such as weather and water conditions contribute to unpredictable load fluctuations that can introduce hydration–dehydration cycling and variable thermal gradients.

Results also suggest that the ESS could play a key role in mitigating these stressors by absorbing high frequency load changes, allowing the PEMFC to operate within a narrower and more stable power band. In these regards, the integration of health-aware energy management strategies tailored to maritime PEMFC/ESS hybrid systems could significantly prolong the operational lifetime of the PEMFC, as supported by the reduced degradation rate shown by the MEA aged under constant load used as a benchmark in this study.

Overall, the proposed methodology provides the preliminary foundation for the development of future maritime PEMFCs durability protocols. Future work should extend this approach to other vessel types and full-stack configurations to provide insights for the development of mitigation and health-aware energy management strategies tailored to ship energy systems. Repeating tests over different types of MEAs, and including post-mortem analysis to retrieve changes in catalyst particle size distribution, could provide additional insights in these regards. Moreover, the combined effect of other unique maritime degradation factors, such as contamination from sodium chloride (NaCl) for ships operating at sea, should be integrated into future tailored ASTs.

CRedit authorship contribution statement

Sara Tamburello: Writing – original draft, Visualization, Validation, Methodology, Investigation, Formal analysis, Data curation, Conceptualization. **Marco Russo Cirillo:** Writing – original draft, Visualization, Validation, Investigation, Formal analysis, Data curation. **Yurii Yakovlev:** Resources, Investigation. **Iva Matolínová:** Writing – review & editing, Supervision, Project administration, Funding acquisition. **Rodolfo Taccani:** Supervision, Project administration. **Andrea Corradu:** Writing – review & editing, Supervision, Project administration, Funding acquisition. **Marco Bogar:** Writing – review & editing, Supervision, Methodology, Investigation, Formal analysis. **Lindert van Biert:** Writing – review & editing, Supervision, Conceptualization.

Declaration of competing interest

The authors declare that they have no known competing financial interests or personal relationships that could have appeared to influence the work reported in this paper.

Acknowledgments

This publication is part of the project SEANERGETIC (with project number KICH1.KICH1.21.003) of the research program Zero Emission and Circular Shipping (KIC), funded by the Dutch Research Council (NWO). This work was also funded by the Johannes Amos Comenius Programme (project number CZ.02.01.01/00/22_008/0004617), call Excellent Research. The authors acknowledge the CERIC-ERIC Consortium for access to experimental facilities (fast-track proposal 20247250 scheduled at the Fuel Cell - Hydrogen Technology Centre at Charles University of Prague).

Appendix A. Supplementary data

Supplementary material related to this article can be found online at <https://doi.org/10.1016/j.electacta.2026.148267>.

Data availability

Data will be made available on request.

References

- [1] IMO, 2023 imo strategy on reduction of ghg emissions from ships, 2023, URL <https://www.imo.org/en/ourwork/environment/pages/2023-imo-strategy-on-reduction-of-ghg-emissions-from-ships.aspx>.
- [2] T. Tronstad, H. Åstrand, G. Haugom, L. Langfeldt, Study on the use of fuel cells in shipping, 2017.
- [3] L. Van Biert, M. Godjevac, K. Visser, P.V. Aravind, A review of fuel cell systems for maritime applications, *J. Power Sources* 327 (2016) 345–364.
- [4] L. Van Biert, K. Mrozewski, P. Hart, Public Final Report: Inventory of the Application of Fuel Cells in The Maritime Sector (FCMAR), Maritime Knowledge Centre (MKC), London, UK, 2021.
- [5] A.G. Elkafas, M. Rivarolo, E. Gadducci, L. Magistri, A.F. Massardo, Fuel cell systems for maritime: A review of research development, commercial products, applications, and perspectives, *Processes* 11 (1) (2023) 97.
- [6] C. Dall'Armi, D. Pivetta, R. Taccani, Hybrid PEM fuel cell power plants fuelled by hydrogen for improving sustainability in shipping: state of the art and review on active projects, *Energies* 16 (4) (2023) 2022.
- [7] H. Fan, N. Abdussamie, P.S.-L. Chen, A. Harris, E.M. Gray, E. Arzaghi, P. Bhaskar, J.A. Mehr, I. Peneisis, Two decades of hydrogen-powered ships (2000–2024): Evolution, challenges, and future perspectives, *Renew. Sustain. Energy Rev.* 219 (2025) 115878.
- [8] J. Wu, X.Z. Yuan, J.J. Martin, H. Wang, J. Zhang, J. Shen, S. Wu, W. Merida, A review of PEM fuel cell durability: Degradation mechanisms and mitigation strategies, *J. Power Sources* 184 (1) (2008) 104–119.
- [9] A. Broer, H. Polinder, L. van Biert, Polymer electrolyte membrane fuel cell degradation in ships—Review of degradation mechanisms and research gaps, *J. Power Sources* 640 (2025) 236678.
- [10] H. Chen, Z. Song, X. Zhao, T. Zhang, P. Pei, C. Liang, A review of durability test protocols of the proton exchange membrane fuel cells for vehicle, *Appl. Energy* 224 (2018) 289–299.
- [11] J. Zhao, X. Li, A review of polymer electrolyte membrane fuel cell durability for vehicular applications: Degradation modes and experimental techniques, *Energy Convers. Manage.* 199 (2019) 112022.
- [12] I. Bloom, L.K. Walker, J.K. Basco, T. Malkow, A. Saturnio, G. De Marco, G. Tsoitridis, A comparison of fuel cell testing protocols—a case study: protocols used by the US Department of Energy, European union, international electrochemical commission/fuel cell testing and standardization network, and fuel cell technical team, *J. Power Sources* 243 (2013) 451–457.
- [13] X.-Z. Yuan, H. Li, S. Zhang, J. Martin, H. Wang, A review of polymer electrolyte membrane fuel cell durability test protocols, *J. Power Sources* 196 (22) (2011) 9107–9116.
- [14] G. Tsoitridis, A. Pilenga, G. De Marco, T. Malkow, et al., EU Harmonised Test Protocols for PEMFC MEA Testing in Single Cell Configuration for Automotive Applications, Publications Office of the European Union Luxembourg, 2015.
- [15] V. Shagar, S.G. Jayasinghe, H. Enshaei, Effect of load changes on hybrid shipboard power systems and energy storage as a potential solution: A review, *Inventions* 2 (3) (2017) 21.
- [16] N.I. Vasilikis, R.D. Geertsma, K. Visser, Operational data-driven energy performance assessment of ships: the case study of a naval vessel with hybrid propulsion, *J. Mar. Eng. Technol.* 22 (2) (2023) 84–100.
- [17] P. Pei, Y. Meng, D. Chen, P. Ren, M. Wang, X. Wang, Lifetime prediction method of proton exchange membrane fuel cells based on current degradation law, *Energy* 265 (2023) 126341.
- [18] H. Choi, H. Choi, H.J. Choi, J. Kim, O.-H. Kim, Y. Kim, S.Y. Sung, D. Eom, S. Park, C.-Y. Ahn, et al., Polymer electrolyte membrane fuel cell durability test using ship operation profile: A comparative study with durability test protocols, *J. Power Sources* 632 (2025) 236396.
- [19] E. Van Sickle, P. Ralli, J. Pratt, L. Klebanoff, MV sea change: The first commercial 100% hydrogen fuel cell passenger ferry in the world, *Int. J. Hydrog. Energy* 105 (2025) 389–404.
- [20] Y.V. Yakovlev, Y.V. Lobko, M. Vorokhta, J. Nováková, M. Mazur, I. Matolínová, V. Matolín, Ionomer content effect on charge and gas transport in the cathode catalyst layer of proton-exchange membrane fuel cells, *J. Power Sources* 490 (2021) 229531.
- [21] Y.V. Yakovlev, M.G. Rodríguez, Y.V. Lobko, M. Vorokhta, P. Kúš, I. Matolínová, V. Matolín, Characterization of gas diffusion layer transport properties by limiting current approach, *Electrochim. Acta* 404 (2022) 139755.
- [22] A.M. Bassam, A.B. Phillips, S.R. Turnock, P.A. Wilson, An improved energy management strategy for a hybrid fuel cell/battery passenger vessel, *Int. J. Hydrog. Energy* 41 (47) (2016) 22453–22464.
- [23] H. Yuan, H. Dai, P. Ming, X. Wang, X. Wei, Quantitative analysis of internal polarization dynamics for polymer electrolyte membrane fuel cell by distribution of relaxation times of impedance, *Appl. Energy* 303 (2021) 117640.
- [24] B. Padha, S. Verma, P. Mahajan, S. Arya, Electrochemical impedance spectroscopy (EIS) performance analysis and challenges in fuel cell applications, *J. Electrochem. Sci. Technol.* 13 (2) (2022) 167–176.
- [25] F. Ciucci, C. Chen, Analysis of electrochemical impedance spectroscopy data using the distribution of relaxation times: A Bayesian and hierarchical Bayesian approach, *Electrochim. Acta* 167 (2015) 439–454.

- [26] T.H. Wan, M. Saccoccio, C. Chen, F. Ciucci, Influence of the discretization methods on the distribution of relaxation times deconvolution: Implementing radial basis functions with drttools, *Electrochim. Acta* 184 (2015) 483–499.
- [27] M. Schönleber, E. Ivers-Tiffée, The distribution function of differential capacity as a new tool for analyzing the capacitive properties of lithium-ion batteries, *Electrochem. Commun.* 61 (2015) 45–48.
- [28] Q. Wang, Z. Hu, L. Xu, J. Li, Q. Gan, X. Du, M. Ouyang, A comparative study of equivalent circuit model and distribution of relaxation times for fuel cell impedance diagnosis, *Int. J. Energy Res.* 45 (11) (2021) 15948–15961.
- [29] I. Pivac, Q. Meyer, C. Zhao, F. Barbir, Operando investigations of proton exchange membrane fuel cells performance during air interruptions in dry and humidified conditions, *J. Power Sources* 580 (2023) 233418.
- [30] M. Heinzmann, A. Weber, E. Ivers-Tiffée, Advanced impedance study of polymer electrolyte membrane single cells by means of distribution of relaxation times, *J. Power Sources* 402 (2018) 24–33.
- [31] Y. Shen, C. Chang, J. Fu, X. Sun, Exploration of relaxation time for the characterization of PEMFC by electrochemical impedance spectroscopy and extended irreversible thermodynamics, *Chem. Eng. J.* 510 (2025) 161561.
- [32] J.-L. Dellis, Zfit, 2025, <https://www.mathworks.com/matlabcentral/fileexchange/19460-zfit>. [Online]; (Accessed 4 June 2025).
- [33] T.T. Cheng, E. Rogers, A.P. Young, S. Ye, V. Colbow, S. Wessel, Effects of crossover hydrogen on platinum dissolution and agglomeration, *J. Power Sources* 196 (19) (2011) 7985–7988.
- [34] A. Weiß, S. Schindler, S. Galbiati, M.A. Danzer, R. Zeis, Distribution of relaxation times analysis of high-temperature PEM fuel cell impedance spectra, *Electrochim. Acta* 230 (2017) 391–398.
- [35] M. Bogar, Y. Yakovlev, S. Pollastri, R. Biagi, H. Amenitsch, R. Taccani, I. Matolínová, Capabilities of a novel electrochemical cell for operando XAS and SAXS investigations for PEM fuel cells and water electrolyzers, *J. Power Sources* 615 (2024) 235070.
- [36] J.A. Gilbert, N.N. Kariuki, X. Wang, A.J. Kropf, K. Yu, D.J. Groom, P.J. Ferreira, D. Morgan, D.J. Myers, Pt catalyst degradation in aqueous and fuel cell environments studied via in-operando anomalous small-angle X-ray scattering, *Electrochim. Acta* 173 (2015) 223–234.
- [37] S. Situ, Humidity-induced degradation mapping of Pt, *Small* 20 (2024) 2407591.
- [38] N. Bevilacqua, M. Schmid, R. Zeis, Understanding the role of the anode on the polarization losses in high-temperature polymer electrolyte membrane fuel cells using the distribution of relaxation times analysis, *J. Power Sources* 471 (2020) 228469.
- [39] Y. Shao, L. Xu, L. Xu, X. Zhang, Z. Wang, G. Zhao, Z. Hu, J. Li, M. Ouyang, Water management issues during load cycling under high temperature and low humidity conditions relevant for heavy-duty applications of PEMFC, *ETransportation* 18 (2023) 100285.
- [40] H. Yuan, H. Dai, P. Ming, L. Zhao, W. Tang, X. Wei, Understanding dynamic behavior of proton exchange membrane fuel cell in the view of internal dynamics based on impedance, *Chem. Eng. J.* 431 (2022) 134035.
- [41] A. Kusoglu, A.M. Karlsson, M.H. Santare, S. Cleghorn, W.B. Johnson, Mechanical behavior of fuel cell membranes under humidity cycles and effect of swelling anisotropy on the fatigue stresses, *J. Power Sources* 170 (2) (2007) 345–358.
- [42] J. Peron, A. Mani, X. Zhao, D. Edwards, M. Adachi, T. Soboleva, Z. Shi, Z. Xie, T. Navessin, S. Holdcroft, Properties of Nafion® NR-211 membranes for PEMFCs, *J. Membr. Sci.* 356 (1–2) (2010) 44–51.
- [43] Q. Yan, H. Toghiani, H. Causey, Steady state and dynamic performance of proton exchange membrane fuel cells (PEMFCs) under various operating conditions and load changes, *J. Power Sources* 161 (1) (2006) 492–502.
- [44] N. Ge, R. Banerjee, D. Muirhead, J. Lee, H. Liu, P. Shrestha, A. Wong, J. Jankovic, M. Tam, D. Susac, et al., Membrane dehydration with increasing current density at high inlet gas relative humidity in polymer electrolyte membrane fuel cells, *J. Power Sources* 422 (2019) 163–174.
- [45] P.C. Okonkwo, O.O. Ige, P.C. Uzoma, W. Emori, A. Benamor, A.M. Abdullah, et al., Platinum degradation mechanisms in proton exchange membrane fuel cell (PEMFC) system: A review, *Int. J. Hydrog. Energy* 46 (29) (2021) 15850–15865.
- [46] S. Ohyagi, T. Sasaki, Durability of a PEMFC Pt–Co cathode catalyst layer during voltage cycling tests under supersaturated humidity conditions, *Electrochim. Acta* 102 (2013) 336–341.
- [47] K. Eom, Y.Y. Jo, E. Cho, T.-H. Lim, J.H. Jang, H.-J. Kim, B.K. Hong, J.H. Lee, Effects of residual oxygen partial pressure on the degradation of polymer electrolyte membrane fuel cells under reverse current conditions, *J. Power Sources* 198 (2012) 42–50.
- [48] R. Borup, J. Meyers, B. Pivovar, Y.S. Kim, R. Mukundan, N. Garland, D. Myers, M. Wilson, F. Garzon, D. Wood, et al., Scientific aspects of polymer electrolyte fuel cell durability and degradation, *Chem. Rev.* 107 (10) (2007) 3904–3951.
- [49] S. Jomori, N. Nonoyama, T. Yoshida, Analysis and modeling of PEMFC degradation: Effect on oxygen transport, *J. Power Sources* 215 (2012) 18–27.
- [50] Y. Zhang, X. Li, A. Klinkova, Numerical investigation of delamination onset and propagation in catalyst layers of PEM fuel cells under hygrothermal cycles, *Int. J. Hydrog. Energy* 46 (19) (2021) 11071–11083.
- [51] A. Perego, A. Avid, D.N. Mamanía, Y. Chen, P. Atanassov, H. Yildirim, M. Odgaard, I.V. Zenyuk, Investigation of cathode catalyst layer interfaces evolution during accelerated stress tests for polymer electrolyte fuel cells, *Appl. Catal. B* 301 (2022) 120810.
- [52] I. Martens, R. Chattot, J. Drnec, Decoupling catalyst aggregation, ripening, and coalescence processes inside operating fuel cells, *J. Power Sources* 521 (2022) 230851.
- [53] M. Bogar, Y. Yakovlev, D.J.S. Sandbeck, S. Cherevko, I. Matolínová, H. Amenitsch, I. Khalakhan, Interplay among dealloying, ostwald ripening, and coalescence in Pt X Ni100–X bimetallic alloys under fuel-cell-related conditions, *ACS Catal.* 11 (18) (2021) 11360–11370.
- [54] T. Yin, D. Chen, T. Hu, S. Hu, R. Li, T. Wei, Y. Li, Y. Li, X. Xu, P. Pei, Experimental investigation and comprehensive analysis of performance and membrane electrode assembly parameters for proton exchange membrane fuel cell at high operating temperature, *Energy Convers. Manage.* 315 (2024) 118740.
- [55] Q. Meyer, Y. Zeng, C. Zhao, Electrochemical impedance spectroscopy of catalyst and carbon degradations in proton exchange membrane fuel cells, *J. Power Sources* 437 (2019) 226922.